International Journal of Applied Engineering Research ISSN 0973-4562 Volume 14, Number 16 (2019) pp. 3552-3565
© Research India Publications. http://www.ripublication.com

Electro-osmotic and Hall Current Effects on the Nanofluid Flow through Porous Medium with Wall Properties

Nabil T. M. El-dabe, Galal M. Moatimid[1], Mohamed A. Hassan[2] and Wessam A. Godh[3]

Department of Mathematics, Faculty of Education, Ain Shams University, Cairo, Egypt.

Corresponding author

Abstract

The current paper investigates the electro-osmotic flow and Hall currents, together with the wall properties and slip condition in magnetohydrodynamic (MHD) peristaltic transport of a nanofluid through a porous medium. The governing equations of motion are analytically solved by using an approximation of the long wavelength and low Reynolds number. The analytical solution is obtained for the velocity of the fluid flow, temperature, nanoparticle concentration, stream function, and the pressure gradient. Moreover, the expressions for volumetric flow rate, skin friction coefficient, Nusselt number, and Sherwood number are given and analyzed. The effects of the physical parameters of the problem with these solutions are discussed and illustrated through a set of figures. The effects of the electro-osmotic parameter, Hall parameter and wall compliant parameters of the fluid reveal many interesting features. It is found that the streamlines form closed loops, creating a cellular flow pattern in the channel and the trapped bolus decreases as the electro-osmotic parameter increases. In contrast, the trapped bolus is increasing with the increase of the Hall parameter.

Keywords: Nanofluid; Peristalsis; Slip conditions; Hall currents; Ion slip; Wall properties; Porous media; Electro-osmotic.

1. INTRODUCTION

Peristaltic pumping is a form of material transport induced by the propagation of waves along the flexible walls of the channel / tube. This is a natural process for the transport of various physiological fluids. This phenomenon has been clarified in details by different researchers; for instance, Fung and Yih [1], and Yin and Fung [2]. Misra and Maiti [3] studied the pumping characteristics during blood flow via the peristaltic mechanism through the vessels of the micro-circulatory system, having varying cross-section. This study of Misra and Maiti [3] was based on using the long wavelength approximation as in the present article, but Fung and Yih [1] and Yin and Fung [2] without using the approximation. An important utilization of peristalsis in stabilizing the blood flow, thus reduces the danger of heart attack and stroke (caused by blood coagulate). The significance of magnetohydrodynamics (MHD) in blood flow through arteries is quite prevalent. Different researchers already analyzed peristalsis with MHD. Furthermore, MHD flows in the presence of Hall current find its applications in MHD generators, flight MHDs and in Hall accelerators. Few attempts for Hall effect on peristalsis can be seen through Refs. [4, 5, and 6]. Hayat et al. [4] studied the Hall current and Joule heating effects on the peristaltic flow of viscous fluid in a channel with flexible walls and observed that both axial and transverse velocities are increasing functions of Hall parameter. This investigation was based on applying the long wavelength and low Reynolds number considerations like the present article but they used the shooting numerical method with fourth-order Runge-Kutta integration. Moreover, Hayat et al. [5] investigated the effects of Hall current and slip conditions on the peristaltic transport of Cu-water nanofluid and showed that Hartman number and Hall parameter have similar effects of velocities and temperature in this case. Furthermore, Abdellateef et al. [6] investigated the influences of Hall currents and heat transfer on peristaltic transport of a nanofluid in a vertical porous tapered channel through a porous medium and observed that the size of the trapped bolus reduces with an increase in the Hall parameter. Although the previous studies [5] and [6] studied the Hall current effects like the present article, the present article added and studied the electro-osmotic flow due to its importance in all of the include systems with highly charged surfaces.

Nanofluids are fluids that contain particles of nanometer size. These particles are termed as nanoparticles. Undoubtedly, the nanofluids are used in many biomedical applications, industrial and engineering. Nanoliquids are utilized in automobiles as coolant, microchips in the computer, fuel cells, surgery, cancer treatment, protein engineering, Photodynamic therapy, drug delivery, water purification, and many others. The pioneering concept of nanofluids was initiated by Choi and Eastman [7], where they tried to suspend various metal and metal oxide nanoparticles in various base fluids. Their results regarding conductivity analysis were promising; however, many things remain elusive about these suspensions of nano-structured materials. Fundamentally, there are two techniques used to produce nanofluids; which are the single-step and the two-step methods [8]. Both of these methods have advantages and disadvantages, which are discussed by Wang and Mujumdar [9]. Due to the important applications and involvement of nanofluids in our daily life, this topic is attracted by scientists and engineers. Some literature in this direction can be seen via Refs. [10, and 11]. Because of the various physiological applications of the flow in a compliant channel and as a

[1] E-mail address: gal_moa @ hotmail.com.
[2] E-mail address: m_a_Hassan_gk @ hotmail.com.
[3] E-mail address: al_ostaz_y2k @ yahoo.com.

difference from the previous researches [10] and [11], the present article has analyzed the effects of the wall properties and studied its effects in the pressure gradient.

Electro-osmotic flow refers to the electrically-driven transport of a fluid relative to the stationary charged surfaces which bound it; for instance, micro-channel walls. It is usually used in chemical analysis, microfluidic devices, and soil analysis and processing, and all of which routinely include systems with highly charged surfaces, often of oxides. Tripathi et al. [12] examined the electro-osmotic peristaltic transport of aqueous nanofluids in a two-dimensional micro-channel analytically and investigated that the decrease of Debye electro-osmotic length considerably accelerates the axial flow. Ranjit and Shit [13] analyzed the entropy generation on electro-osmotic flow pumping by a uniform peristaltic wave. This study puts an important observation that the entropy generation number attains the maximum value in the region close to the walls of the channel, while it gains minimum value near the central region of the channel. The same approximation of Debye-Hückel linearization that was applied by Tripathi et al. [12] and Ranjit and Shit [13] is used in the present study.

The flow in a compliant channel is important because of its various physiological applications such as air flow in the lungs, blood flow in arteries and veins and urine stream in the urethras. Iftikhar et al. [14] considered the influence of wall properties and Cu-water nanofluid in a non-uniform inclined tube. They observed that the temperature profile decreases by increasing values of the nanoparticle volume fraction. This justifies the use of the nanoparticle in different type as a coolant. Hayat et al. [15] explored the peristaltic flow of Williamson nanofluid in an endoscope with partial slip and wall properties. They investigated that the fluid velocity shows an increasing behavior with the wall parameters E_1 and E_2, while for E_3, the situation is reversed. In order to study the effects of electro-osmotic flow due to its importance and applications in chemical analysis, and also the importance of Hall current effects and its applications in heat transfer, the present investigation added the studied of their effects besides the influence of wall properties.

No slip boundary condition does not remain valid in problems dealing with the polishing of artificial heart valves, thin film, rarefied fluid and fluid motion within the human body,… etc. It is well accepted that the slip effects may appear for two types of fluids such as rarefied gases and fluids that having much more elastic character. In these fluids, slippage appears as a result of large tangential traction. In general, in the study of fluid-solid surface interactions, the concept of the slip of a fluid at a solid wall serves to describe macroscopic effects of certain molecular phenomena. Hayat et al. [16] studied the effect of slip conditions on the peristaltic transport of copper-water nanofluid. They investigated that both axial and transverse velocities increase for a large value of slip parameters. Ramesh [17] investigated the effects of slip and convective conditions on the peristaltic flow of couple stress fluid in an asymmetric channel through a porous medium. One of the important results of this investigation is that the increasing slip parameter increases the velocity near the boundary of the walls and Brinkman number increases the temperature of the fluid. In the present article, only the velocity slip condition was taken into account. But, Hayat et al. [16] considered the thermal slip condition besides the velocity slip condition. Meanwhile, the effect of Biot number on the temperature was discussed by Ramesh [17].

In light of the above discussion, the present work aims to analyze the effects of the electro-osmotic flow, the Hall current, wall properties, and slip conditions of MHD peristaltic transport of a nanofluid. The permeability of the fluid is taken into account. The analysis is performed under long wavelength and low Reynolds number approximations. The governing equations of motion are analytically solved. The distributions of the stream function, the axial velocity, temperature, concentration, volumetric flow rate, skin friction coefficient, Nusselt number, and Sherwood number are obtained as functions of the physical parameters of the problem. The effects of these parameters on the obtained solutions are numerically discussed and graphed throughout a set of figures. To clarify the manuscript, the remainder of the article is organized as follows: In Section 2, a formulation of the problem is presented. In Section 3, the method of solution is presented. The discussion of the results is illustrated in Section 4. Finally, in Section 5, concluding remarks of the outcomes are drawn.

2. FORMULATION OF THE PROBLEM

A two-dimensional flexible permeable channel of uniform thickness is considered. The walls of the channel are taken as a stretched membrane, on which the traveling sinusoidal wave of moderate amplitude is imposed. The following assumptions are made in this investigation:

- The characteristic properties of the two-dimensional flow depend on the Cartesian coordinates (x, y), where the flow direction is horizontally taken on the x-axis and the y-axis is vertical.
- For simplicity, an axisymmetric type of motion is assumed at which the gravitational forces are neglected under the assumption of a horizontal motion as a facilitator of the solution.
- The Hall currents and ion slip effects are taken into account by applying a strong uniform magnetic field with magnetic flux density $\underline{B} = (0,0,B_0)$.
- The electro-osmotic flow arises due to the supplied electric field E_x parallel to the channel walls. Therefore, the electrical double layer (EDL) is formed from the positive (cations) and negative (anions) ions which cause electro-osmotic flow (EOF) through the channel [18].

The description of the problem is sketched in Fig.1 along with the above consideration. The channel wall geometry is represented as:

$$\eta(x,t) = d(x) + a\sin\frac{2\pi}{\lambda^*}(x - c^*t), \tag{1}$$

where $d(x) = d + Q^*x, \quad Q^* \ll 1.$

If the Hall and ion slip terms are retained in the generalized Ohm's law, the current density $\underline{J}$ is given by [19, 20]

$$\underline{J}=\sigma\left(\underline{E}+\underline{V}\times\underline{B}-\beta^{*}(\underline{J}\times\underline{B})+\frac{\beta^{*}\beta_{i}}{B_{0}}(\underline{J}\times\underline{B})\times\underline{B}\right), \quad (2)$$

where $\underline{E}$ is the electric field which results from a charge separation in the $z-$direction, β^{*} is the Hall factor, and β_{i} is the ion slip parameter.

Thus, in terms of Eq. (2) and under the previous assumptions the basic equations that are governing the motion become as following:

The incompressibility conditions yields

$$\frac{\partial u}{\partial x}+\frac{\partial v}{\partial y}=0, \quad (3)$$

The conversation of momentum gives

$$\rho\left(\frac{\partial u}{\partial t}+u\frac{\partial u}{\partial x}+v\frac{\partial u}{\partial y}\right)=\frac{\partial p}{\partial x}+\mu\left(\frac{\partial^{2}u}{\partial x^{2}}+\frac{\partial^{2}u}{\partial y^{2}}\right)-$$
$$-\frac{\mu}{K}u-\frac{\sigma B_{0}^{2}(1+\beta_{i}\beta_{e})u}{(1+\beta_{i}\beta_{e})^{2}+B_{e}^{2}}+\frac{(\sigma B_{0}^{2}\beta_{e}\beta^{*})v}{(1+\beta_{i}\beta_{e})^{2}+B_{e}^{2}}+\rho_{e}E_{x} \quad (4)$$

and

$$\rho\left(\frac{\partial v}{\partial t}+u\frac{\partial v}{\partial x}+v\frac{\partial v}{\partial y}\right)=$$
$$-\frac{\partial p}{\partial y}+\mu\left(\frac{\partial^{2}v}{\partial x^{2}}+\frac{\partial^{2}v}{\partial y^{2}}\right)-\frac{\mu}{K}v \quad (5)$$
$$-\frac{\sigma B_{0}^{2}(1+\beta_{i}\beta_{e})v}{(1+\beta_{i}\beta_{e})^{2}+B_{e}^{2}}+\frac{(\sigma B_{0}^{2}\beta_{e}\beta^{*})u}{(1+\beta_{i}\beta_{e})^{2}+B_{e}^{2}},$$

The conversation of energy results

$$\frac{\partial T}{\partial t}+u\frac{\partial T}{\partial x}+v\frac{\partial T}{\partial y}=\frac{k}{\rho c_{f}}\left(\frac{\partial^{2}T}{\partial x^{2}}+\frac{\partial^{2}T}{\partial y^{2}}\right)+$$
$$+\frac{\rho_{p}c_{p}}{\rho c_{f}}\left(D_{B}\left(\frac{\partial C}{\partial x}\frac{\partial T}{\partial x}+\frac{\partial C}{\partial y}\frac{\partial T}{\partial y}\right)+\frac{D_{T}}{T_{0}}\left((\frac{\partial T}{\partial x})^{2}+(\frac{\partial T}{\partial y})^{2}\right)\right), \quad (6)$$

The concentration equation presents

$$\frac{\partial C}{\partial t}+u\frac{\partial C}{\partial x}+v\frac{\partial C}{\partial y}=D_{B}\left(\frac{\partial^{2}C}{\partial x^{2}}+\frac{\partial^{2}C}{\partial y^{2}}\right)+\frac{D_{T}}{T_{0}}\left(\frac{\partial^{2}T}{\partial x^{2}}+\frac{\partial^{2}T}{\partial y^{2}}\right), \quad (7)$$

from the Gaussian law, one gets

$$\nabla\cdot\underline{E}=\frac{\rho_{e}}{\gamma}, \quad (8)$$

$$\underline{E}=-\nabla\phi, \quad (9)$$

Combining Eqs. (8) and (9), Poisson equation for the electrical potential distribution may be given as

$$\nabla^{2}\phi=-\nabla\cdot\underline{E}=-\frac{\rho_{e}}{\gamma}, \quad (10)$$

For a symmetric electrolyte, the ions and the counter ions have the same charge valence,

$z_{+}=-z_{-}=z,$ where z is the valence number of ions.

The total electric charge density is given by [18]

$$\rho_{e}=ez(n_{+}-n_{-}), \quad (11)$$

To obtain the potential distribution, it is necessary to describe the density of the charge number. This is done by applying the Nernst–Planck equation [21] as

$$\frac{\partial n_{\pm}}{\partial t}+u\frac{\partial n_{\pm}}{\partial x}+v\frac{\partial n_{\pm}}{\partial y}=$$
$$D\left(\frac{\partial^{2}n_{\pm}}{\partial x^{2}}+\frac{\partial^{2}n_{\pm}}{\partial y^{2}}\right)\pm\frac{Dze}{K_{B}T_{m}}\left(\frac{\partial}{\partial x}(n_{\pm}\frac{\partial\varphi}{\partial x})+\frac{\partial}{\partial y}(n_{\pm}\frac{\partial\varphi}{\partial y})\right), \quad (12)$$

The compliant wall condition as:

$$\frac{\partial}{\partial x}L^{*}(\eta)=\frac{\partial p}{\partial x}=\mu\left(\frac{\partial^{2}u}{\partial x^{2}}+\frac{\partial^{2}u}{\partial y^{2}}\right)-\rho\left(\frac{\partial u}{\partial t}+u\frac{\partial u}{\partial x}+v\frac{\partial u}{\partial y}\right)$$
$$-\frac{\mu}{K}u-\frac{\sigma B_{0}^{2}(1+\beta_{i}\beta_{e})u}{(1+\beta_{i}\beta_{e})^{2}+B_{e}^{2}}+\frac{(\sigma B_{0}^{2}\beta_{e}\beta^{*})v}{(1+\beta_{i}\beta_{e})^{2}+B_{e}^{2}}+\rho_{e}E_{x}, \quad (13)$$
$$\text{at}\quad y=\pm\eta$$

The appropriate boundary conditions may be listed as follows:

$$T=T_{0},C=C_{0},v=\frac{\partial\eta}{\partial t},\ \text{at}\ y=-\eta(x,t),$$

$$\text{and}\ T=T_{1},C=C_{1},v=-\frac{\partial\eta}{\partial t},\phi=\xi,\ \text{at}\ y=\eta(x,t), \quad (14)$$

In addition, one finds

$$\frac{\partial\phi}{\partial y}=0\ \text{at}\ y=0, \quad (15)$$

The slip conditions at the walls are defined as:

$$\text{at}\ y=\pm\eta(x,t)=\pm\left(d+Q^{*}x+a\sin\frac{2\pi}{\lambda^{*}}(x-c^{*}t)\right), \quad (16)$$

Now, it is convenient to introduce the following non-dimensional quantities:

$$x^{'}=\frac{x}{\lambda^{*}},y^{'}=\frac{y}{d},t^{'}=\frac{ct}{\lambda^{*}},\theta=\frac{T-T_{0}}{T_{1}-T_{0}},$$
$$\Omega=\frac{C-C_{0}}{C_{1}-C_{0}},U_{HS}=\frac{-\gamma\xi E_{x}}{\mu c},\eta^{'}=\frac{\eta}{d},p^{'}=\frac{d^{2}p}{c^{*}\lambda^{*}\mu},$$
$$K^{'}=\frac{K}{d^{2}},\alpha=\frac{k}{\rho c_{f}},N_{b}=\frac{\rho c_{p}D_{B}(c_{1}-c_{0})}{\rho c_{f}\alpha},$$
$$\beta=\frac{h}{d},\varphi^{'}=\frac{\varphi}{\xi},n^{'}=\frac{n}{n_{0}},N_{t}=\frac{\rho c_{p}D_{T}(T_{1}-T_{0})}{\rho c_{f}\alpha T_{0}},$$

$$M^2=\frac{\sigma B_0^2 d^2}{\mu},\nu=\frac{\mu}{\rho},\Pr=\frac{\nu}{\alpha},Sc=\frac{\nu}{D_B},$$
$$R=\frac{c^* d\rho}{\mu},\varepsilon=\frac{a}{d},\delta=\frac{d}{\lambda^*},E_1=\frac{-\tau d^3}{\lambda^{*3}\mu c^*},$$
$$E_2=\frac{m_1^* c^* d^3}{\lambda^{*3}\mu},E_3=\frac{c_v d^3}{\lambda^{*2}\mu},Q=\frac{\lambda^* Q^*}{d},m=d\sqrt{\frac{2ezn_0}{\in\xi}},u'=\frac{u}{c}$$
$$\text{and } v'=\frac{v}{\delta c}. \tag{17}$$

Using the above non-dimensional quantities in equations $(1-16)$ under the assumptions of long wavelength ($\delta \ll 1$) and low Reynolds number approximations, the resulting equations can be written as:

$$\eta(x,t)=1+Qx+\varepsilon\sin 2\pi(x-t), \tag{18}$$

$$\frac{\partial u}{\partial x}+\frac{\partial v}{\partial y}=0, \tag{19}$$

$$\frac{\partial p}{\partial x}=\frac{\partial^2 u}{\partial y^2}-\left(\frac{1}{K}+M^2\frac{(1+\beta_i\beta_e)}{(1+\beta_i\beta_e)^2+B_e^2}\right)u+m^2\phi U_{HS}, \tag{20}$$

$$\frac{\partial p}{\partial y}=0, \tag{21}$$

$$\frac{\partial^2\theta}{\partial y^2}+N_b\frac{\partial\Omega}{\partial y}\frac{\partial\theta}{\partial y}+N_t\left(\frac{\partial\theta}{\partial y}\right)^2=0, \tag{22}$$

$$\frac{\partial^2\Omega}{\partial y^2}+\frac{N_t}{N_b}\frac{\partial^2\theta}{\partial y^2}=0, \tag{23}$$

$$\frac{\partial^2\phi}{\partial y^2}=-m^2\left(\frac{n_+-n_-}{2}\right), \tag{24}$$

$$\text{and}\qquad \frac{\partial^2 n_\pm}{\partial y^2}\pm\frac{\partial}{\partial y}\left(n_\pm\frac{\partial\phi}{\partial y}\right)=0, \tag{25}$$

In addition, the related boundary conditions yield:

$$u=\mp\beta\frac{\partial u}{\partial y}\text{ at } y=\pm\eta(x,t)=\pm\left(1+Qx+\varepsilon\sin 2\pi(x-t),\right) \tag{26}$$

$$\frac{\partial^2 u}{\partial y^2}-\left(\frac{1}{K}+M^2\frac{(1+\beta_i\beta_e)}{(1+\beta_i\beta_e)^2+B_e^2}\right)u+m^2\phi U_{HS}=$$
$$-8\varepsilon\pi^3(E_1+E_2)\cos 2\pi(x-t)+4\varepsilon\pi^2E_3\sin 2\pi(x-t),$$
$$\text{at } y=\pm\eta(x,t) \tag{27}$$

$$\left.\begin{aligned}&\theta(x,y,t)=\Omega(x,y,t)=0,\text{ at } y=-\eta(x,t)\\&\theta(x,y,t)=\Omega(x,y,t)=1,\phi=1,\text{ at } y=\eta(x,t)\\&\frac{\partial\phi}{\partial y}=0,\text{ at } y=0\\&\text{The bulk conditions :}\\&n_\pm=1\text{ at }\phi=0\text{ and }\frac{\partial n_\pm}{\partial y}=0\text{ at }\frac{\partial\phi}{\partial y}=0\end{aligned}\right\} \tag{28}$$

Moreover, it is assumed that the zero value of the streamline at the line $y=0$, [22].

Now, the previous system of Eqs (18-28) will be solved in the next sections.

3. METHOD OF SOLUTION

Equation (25) may be solved subjected to the bulk conditions (28). Therefore, its solution may be written as

$$n_\pm=e^{\mp\phi} \tag{29}$$

Substituting eq. (29) into Eq. (24), one gets

$$\frac{\partial^2\phi}{\partial y^2}=m^2\sinh\phi, \tag{30}$$

Under Debye–Hückel's linearization [21] (i.e. $\xi<25mV$), $\sinh\phi\approx\phi,$ hence,

$$\frac{\partial^2\phi}{\partial y^2}=m^2\phi, \tag{31}$$

The solution for ϕ that satisfies the boundary conditions given in Eq. (28) may be written as

$$\phi=\frac{\cosh my}{\cosh m\eta}, \tag{32}$$

Substituting Eq. (32) into Eq. (20), the resulting partial differential equation may be solved exactly under the compliant wall conditions (27), and the fluid velocity u may be written as follows:

$$u(x,y,t)=\frac{-1}{N^2}\frac{\partial p}{\partial x}-\frac{S_1(x,t)}{m^2-N^2}\cosh(my)+$$
$$+\frac{S_2(x,t)}{2}\sec h(N\eta(x,t))\left(\frac{e^{Ny}}{1-\beta N}+\frac{e^{-Ny}}{1+\beta N}\right), \tag{33}$$

After applying the slip conditions (26) in Eq. (33), one gets:

$$\frac{\partial p}{\partial x}=S_1(x,t)\cosh(my)-m^2U_{HS}-8\varepsilon\pi^3(E_1+E_2)\cos 2\pi(x-t)$$
$$+4\varepsilon\pi^2E_3\sin 2\pi(x-t), \tag{34}$$

where $N^2 = \frac{1}{K} + M^2 \frac{(1+\beta_i\beta_e)}{(1+\beta_i\beta_e)^2 + B_e^2}$,

$S_1(x,t) = \frac{m^2 U_{HS}}{\cosh(m\eta(x,t))}$ and

$S_2(x,t) = \frac{1}{N^2}\frac{\partial p}{\partial x} + \frac{S_1(x,t)}{m^2 - N^2}\cosh(m\eta(x,t)) + m\beta \sec h(m\eta(x,t))$.

Integrating Eq. (23) twice with respect to y, under the boundary conditions given in Eq. (28), one gets

$$\Omega + \frac{N_t}{N_b}\theta = \frac{1}{2}\left(1 + \frac{N_t}{N_b}\right)\left(\frac{1}{\eta(x,t)}y + 1\right), \tag{35}$$

Substituting from Eq. (35) into Eq. (22) and solving the resulting partial differential equation under applying the conditions (28), the solution of the temperature may be written as:

$$\theta(x,y,t) = \frac{-1}{e^{N_1} - 1} + \frac{1}{2}\cosh\frac{1}{2}N_1 e^{N_2(x,t)y}, \tag{36}$$

To get the solution of nanoparticle concentration Ω, from Eq. (36) in Eq. (35), one gets

$$\begin{aligned}\Omega(x,y,t) &= \frac{1}{2\eta(x,t)}\left(1 + \frac{N_t}{N_b}\right)y \\ &+ \frac{1}{2}\left(1 + \frac{N_t}{N_b}\right) - \frac{N_t}{N_b}\left(\frac{-1}{e^{N_1} - 1} + \frac{1}{2}\cosh\frac{1}{2}N_1 e^{N_2(x,t)y}\right),\end{aligned} \tag{37}$$

where $N_1 = \frac{N_b^2}{N_t}\left(1 + \frac{N_t}{N_b}\right)$ and

$N_2(x,t) = \frac{N_b^2}{2\eta(x,t)N_b}\left(1 + \frac{N_t}{N_b}\right)$.

By introducing a stream function ψ such that

$$u = \frac{\partial \psi}{\partial y}. \tag{38}$$

This function ψ may be obtained by integrating Eq. (33) with respect to y, and after applying the assumption condition $\psi(x,0,t) = 0$ the stream function ψ may be written as follows:

$$\begin{aligned}\psi(x,y,t) &= \frac{-1}{N^2}\frac{\partial p}{\partial x}y - \frac{S_1(x,t)}{m(m^2 - N^2)}\sinh(my) + \\ &\frac{S_2(x,t)}{2}\sec h(N\eta(x,t))\left(\frac{e^{Ny}}{N(1-\beta N)} - \frac{e^{-Ny}}{N(1+\beta N)}\right) + \\ &\frac{S_2(x,t)}{2}\sec h(N\eta(x,t))\left(\frac{1}{N(1+\beta N)} - \frac{1}{N(1-\beta N)}\right)\end{aligned} \tag{39}$$

The volumetric flow rate [18], the shear stress (skin friction coefficient), the rate of heat transfer (Nusselt number) and the rate of mass transfer at the wall (Sherwood number) are defined as follows respectively [23]:

$$G(x,t) = \int_0^{\eta(x,t)} u(x,y,t)dy, \tag{40}$$

$$S_f(x,t) = \frac{\partial \eta(x,t)}{\partial x}\frac{\partial u(x,y,t)}{\partial y}\bigg|_{y=\eta(x,t)} \tag{41}$$

$$Nu(x,t) = \frac{\partial \eta(x,t)}{\partial x}\frac{\partial \theta(x,y,t)}{\partial y}\bigg|_{y=\eta(x,t)} \tag{42}$$

$$Sh(x,t) = \frac{\partial \eta(x,t)}{\partial x}\frac{\partial \Omega(x,y,t)}{\partial y}\bigg|_{y=\eta(x,t)} \tag{43}$$

These quantities G, S_f, Nu and Sh may be evaluated numerically by using the Mathematica software.

In what follows, the previous analytical results are depicted to indicate the influences of various parameters.

4. RESULTS AND DISCUSSION

In what follows a numerical estimation will be performed to analyze the mathematical results graphically in Figs. 3–22 for velocity, temperature, nanoparticle concentration distributions, pressure gradient, and volumetric flow rate profiles. The values of the skin friction, Nusselt number and the Sherwood number on the wall are also discussed. Furthermore, the trapping phenomenon is illustrated using the streamline graphs. In the present study the following default parameter values are adopted for computations as follows:

$U_{HS} = 2; m = 1; N_t = 0.1; N_b = 1; M = 0.5; k = 1.2;$
$\varepsilon = 0.5; Q = 1; \beta = 0.06; E_1 = 4; E_2 = 3; E_3 = 2; \beta_i = 0.2$
$; \beta_e = 0.4$. All graphs are therefore correspond to these values unless specifically indicated on the appropriate graph. In addition, it contains a comparison between the present results of the velocity by neglecting the electro-osmotic parameter and neglecting the effects of the Hall currents and ion slip when $U_{HS} = Q = m = \beta_i = \beta_e = 0$ with the previous results that are already obtained by Machireddy and Kattamreddy [23]. The results are compared graphically in Fig. 2. The specific values in this figure are chosen as: $M = 1;\ k = 1;\ \varepsilon = 0.02;\ \beta = 0.1;$ $E_1 = 1;\ E_2 = 0.5;\ E_3 = 0.5;$ in order to compare between the special cases (a) $U_{HS} = Q = m = \beta_i = \beta_e = 0$ and (b) $U_{HS} = Q = 1, m = \beta_i = \beta_e = 2$. Fig. 2 (a) shows a similarity between velocity curves of the present solutions and the previous ones. In addition, Fig. 2 (b) shows that the difference between results increase when U_{HS}, Q, m, β_i and β_e are not approached to zero.

4.1. Streamlines configuration

Fig. 3 illustrates that the trapping bolus gradually disappears with the increase of the electro-osmotic parameter. This implies that the strong applied electric field leads to a regular flow. The

same behavior of the electro-osmotic parameter was illustrated by Moatimid et al. [18]. Fig. 4 displays the streamline patterns and trapping for the value of the Hall parameter β_e. It is explained from this figure that the trapped bolus increases as the Hall parameter β_e is increased.

4.2. The fluid velocity profile

In Fig. 5, it is evident that an increase in electro-osmotic parameter m substantially accelerates the axial flow. Physically, that is occur since the induced electrical field is dwarfed by the externally applied electric field, streaming potential is discarded in the electro-osmotic flow. When the ions move in the diffuse layer, they pull the liquid along with them in the opposite direction to the pressure driven flow. This effect is inversely proportional to the thickness of the electrical double layer [24]. Hence, as my values increase the migration of ions is inhibited and the axial flow is accelerated, as observed in Fig. 5. The same behavior was illustrated by Tripathi et al. [12] and Tripathi et al. [25]. However, it is interesting to note from Fig. 6 that the velocity u in the vicinity of the channel wall increases dramatically with slip parameter β. It is shown that the effects of the wall slip, yield a potential to stop the velocity gradients in the interface region and those effects, drag the advection transport of moving ions in the EDL (Electrical Double Layer). This coupling between the wall slip and EDL transport plays the momentous role in determining the streaming potential field. It is strongly influences the consequent variations in the energy transfer efficiency. Therefore, the slip effect has an important role on the velocity. A similar trend has been reported in Ranjit et al. [26]. It can be seen from Fig. 7 that larger Hall parameter values β_e increase the fluid velocity for large values of m. This behavior is physically holding as larger values of the conductivity β_e decreases which cause decay in the damping force and enhancement in the velocity [27]. The opposite behavior of the fluid velocity is observed for the small values of m. Fig. 8 detected that with an increase in Helmholtz–Smoluchowski velocity U_{HS} i.e. maximum electro osmotic velocity, from 2 to 20, there is initially a strong acceleration in the axial flow. However, for $U_{HS} = 20$ i.e. with subsequent increase in the axial electrical field, there is a significant deceleration induced. A critical electrical field strength there exists beneath which the flow is assisted and above which it is impeded. A similar trend has been reported in Tripathi et al. [12].

4.3. The temperature profile

Fig. 9 and Fig. 10 displayed the effect of the thermophoresis parameter N_t and Brownian parameter N_b on the behavior of temperature profile. The obtained results explain the growing temperature distribution via larger N_t through Fig. 9. Physically, as seen in Mekheimer and Abd Elmaboud [28] the increasing in the temperature distribution of fluid acquires nanoparticles more energy to help in destroying and damaging the tumor tissues (thermotherapy of oncology). The opposite behavior of the temperature profile is observed for the effect of the Brownian parameter N_b as shown in Fig. 10.

4.4. The nanoparticle concentration

From Fig. 11, it is observed that the nanoparticle concentration increases with the increase of thermophoresis parameter N_t. Furthermore, the effect of Brownian parameter N_b in the nanoparticle concentration profile is depicted in Fig. 12. Actually, increasing in this motion parameter N_b means that the density of nanoparticles increased, which results in enhancement of mass flux and thus concentration profile increases [10].

4.5. Pressure gradient profile

The impact of elasticity parameters E_1, E_2 and E_3 in Figs. 13 – 15 are to grow a quantity of pressure difference $\frac{\partial p}{\partial x}$ across the channel. It can be seen from these figures that, in the wider parts of the channel, the pressure gradient is small, that is, the flow can simply go without a load of a great pressure gradient. Nevertheless, in the narrow parts of the channel, a bigger pressure gradient is needed to keep with the same flux to pass it. Ellahi et al. [29] discussed the same behavior for pressure difference across the channel.

4.6. The volumetric flow rate

Fig. 16 depicted that volume flow rate G enhances with reducing the magnitude of EDL thickness (i.e., the value of the electro-osmotic parameter, $m \in [2,3.3]$) in the interval $x \in [1.2,2]$. Otherwise, these curves are very close to each other. Similar behavior has been discussed in Tripathi et al. [21].

4.7. Skin friction coefficient, Nusselt number, and Sherwood number

Figs. 17 and 18 illustrated the impacts of both electro-osmotic parameter m and the ion slip parameter β_i on the skin friction coefficient S_f. It is observed from Fig. 17 that S_f increases with the increase in m in the region $0.2 < x < 0.5$. At the same time, in the region $0.5 < x < 0.8$, the contrary behavior is observed, and otherwise, the curves are very close to each other. Fig. 18 indicates that a decrease in S_f occurs with an increase in β_i. Figs. 19–22 displayed the effects of both the Brownian parameter N_b and thermophoresis parameter N_t on the Nusselt number Nu and Sherwood number Sh. Fig. 19 and Fig. 20 indicated that Nu decreases with the increase of N_t while it increases with the increase of N_b. Fig. 21 and Fig. 22 indicated that a decrease in Sh occurs with an increase in N_b

and N_t. In general, S_f, Nu and Sh profiles obey dual role criterion. Their inflection points occur at $-\eta$, at the centerline of the channel and at η. The same discussion for the dual role has been reported by Moatimid et al. [18].

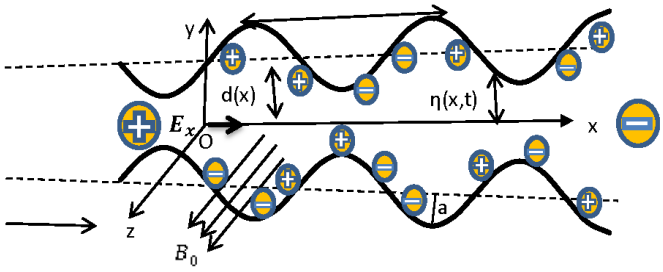

Fig. 1 Geometry of the problem.

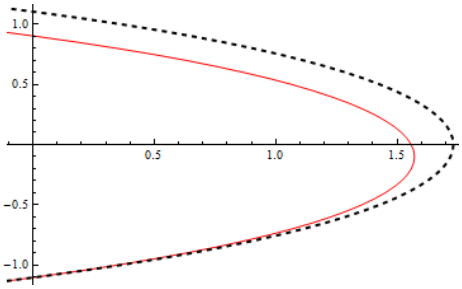

(a) $\mathbf{U_{HS}} = \boldsymbol{Q} = \boldsymbol{m} = \boldsymbol{\beta_i} = \boldsymbol{\beta_e} = \mathbf{0}$

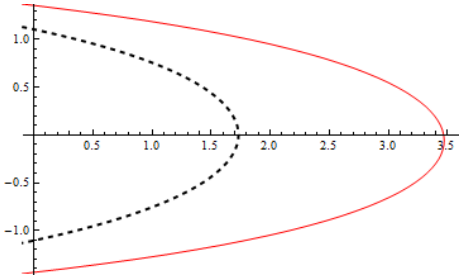

(b) $\mathbf{U_{HS}} = \boldsymbol{Q} = \mathbf{1}, \boldsymbol{m} = \boldsymbol{\beta_i} = \boldsymbol{\beta_e} = \mathbf{2}$.

Fig .2 Plots of velocity $\boldsymbol{u}$ versus $\boldsymbol{y}$

) In the special case in our problem from Eq. (33)———(

(-------) In previous results of Machireddy and Kattamreddy [20]

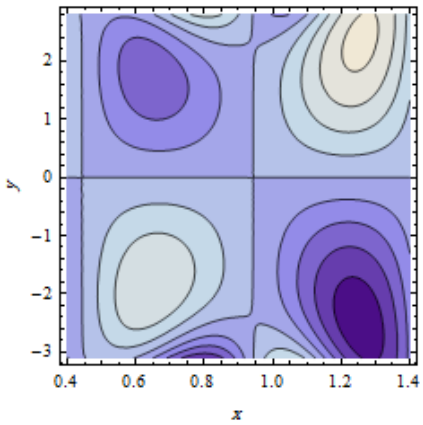

(a) $m = 1$

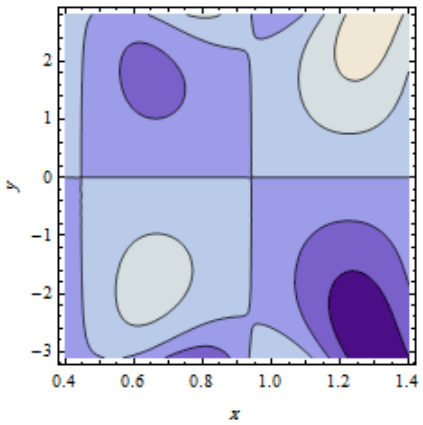

(b) $m = 3$

Fig .3 Plots of Streamline ψ distribution from Eq. (39) for the effects of m.

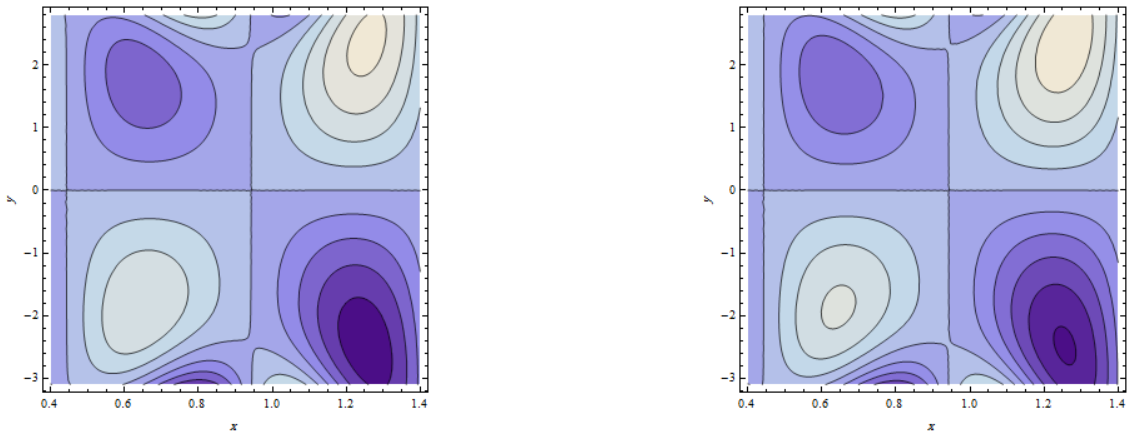

(a) $\beta_e = 0.4$ (b) $\beta_e = 1.8$

Fig .4 Plots of Streamline ψ distribution from Eq. (39) for the effects of β_e.

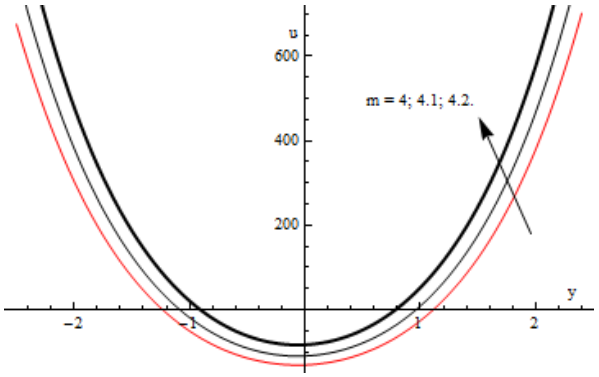

Fig .5 Plots of velocity u versus y from Eq**.** (33) for the effects of m.

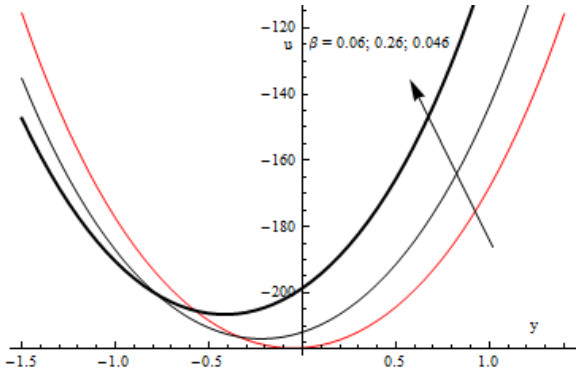

Fig .6 Plots of velocity u versus y from Eq**.** (33) for the effects of β.

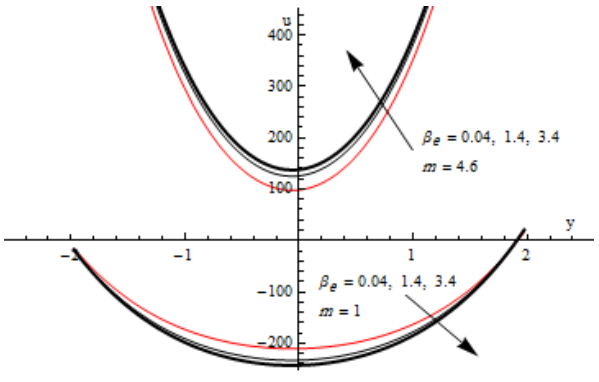

Fig .7 Plots of velocity u versus y from Eq**.** (33) for the effects of β_e.

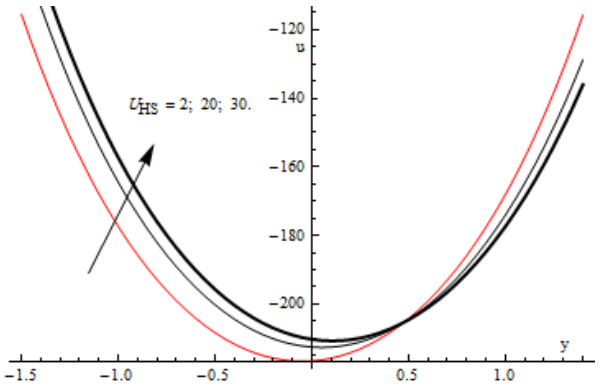

Fig .8 Plots of velocity u versus y from Eq**.** (33) for the effects of U_{HS}.

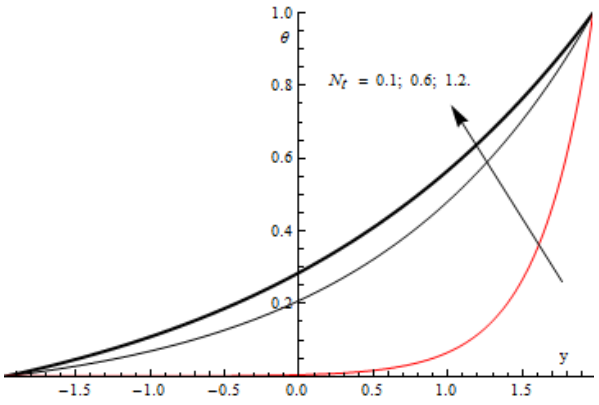

Fig .9 Plots of temperature profile θ versus y from Eq. (36) for the effects of N_t.

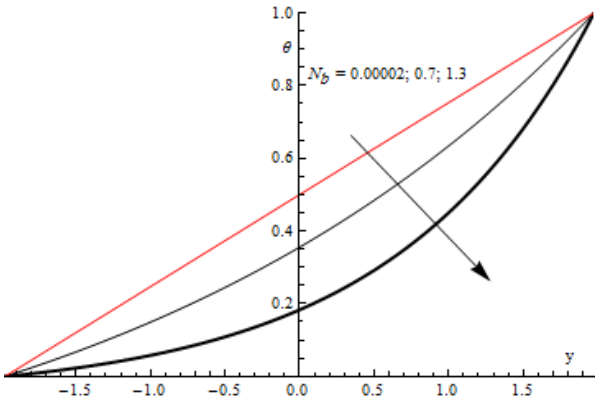

Fig .10 Plots of temperature profile θ versus y from Eq. (36) for the effects of N_b.

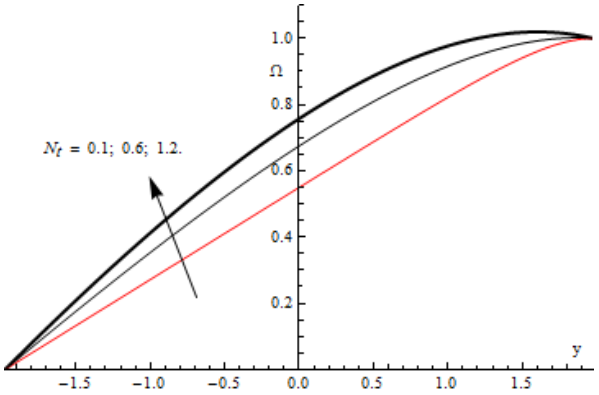

Fig .11 Plots of nanoparticle concentration Ω versus y from Eq. (37) for the effects of N_t.

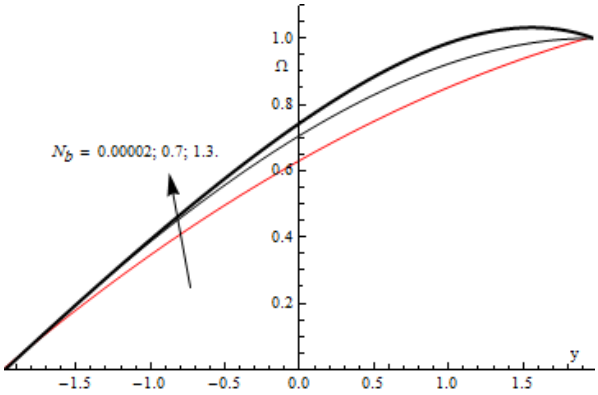

Fig .12 Plots of nanoparticle concentration Ω versus y from Eq. (37) for the effects of N_b.

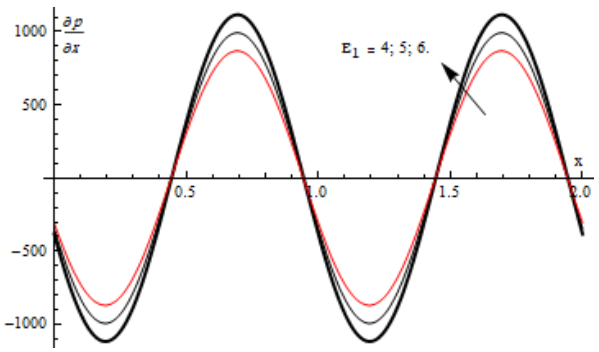

Fig .13 Plots of pressure gradient $\frac{\partial p}{\partial x}$ versus x from Eq. (34) for the effects of E_1.

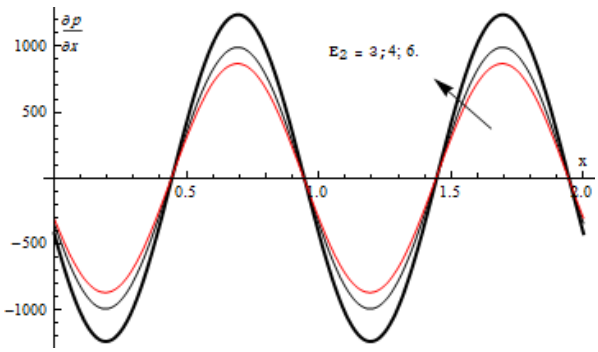

Fig .14 Plots of pressure gradient $\frac{\partial p}{\partial x}$ versus x from Eq. (34) for the effects of E_2.

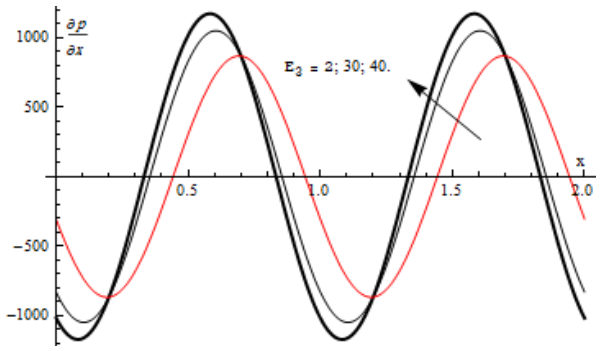

Fig .15 Plots of pressure gradient $\frac{\partial p}{\partial x}$ versus x from Eq. (34) for the effects of E_3.

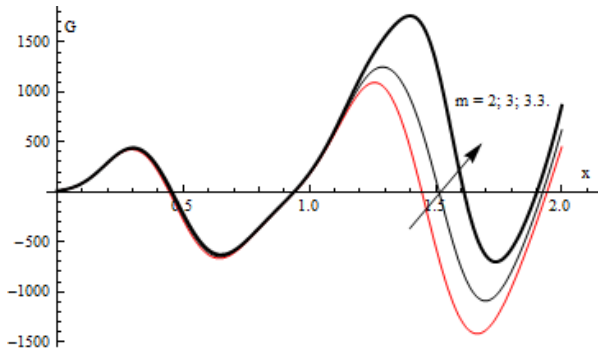

Fig .16 Plots of volumetric flow rate G versus x from Eq. (40) for the effects of m.

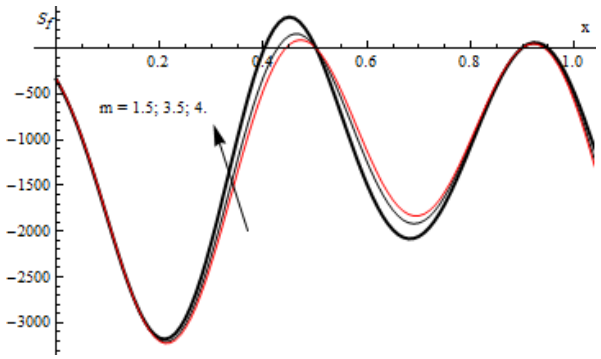

Fig .17 Plots of skin friction S_f versus x from Eq. (41) for the effects of m.

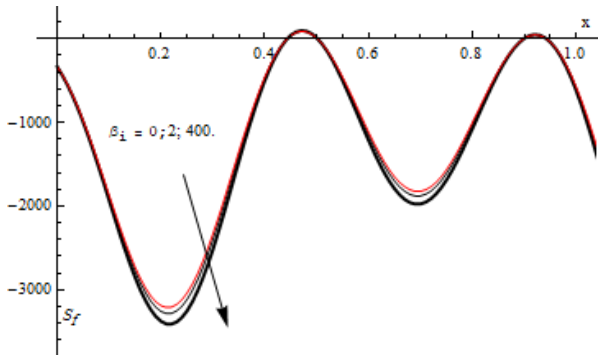

Fig .18 Plots of skin friction S_f versus x from Eq. (41) for the effects of β_i.

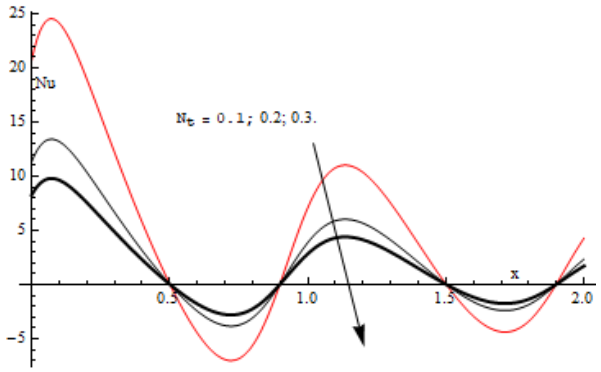

Fig .19 Plots of nusselt number Nu versus x from Eq. (42) for the effects of N_t.

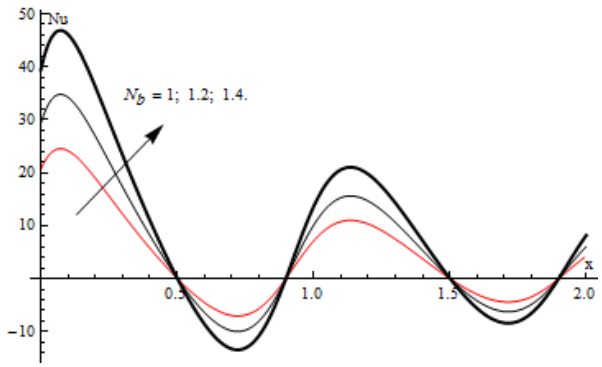

Fig .20 Plots of nusselt number Nu versus x from Eq. (42) for the effects of N_b.

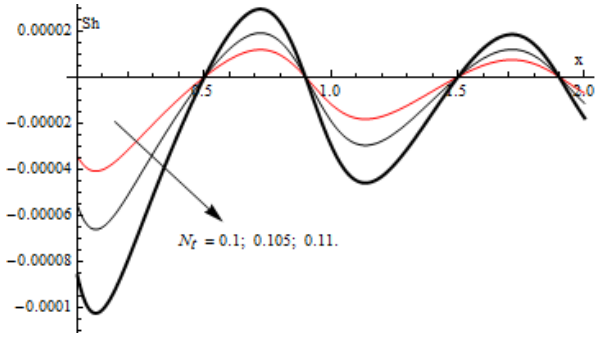

Fig .21 Plots of Sherwood number Sh versus x from Eq. (43) for the effects of N_t.

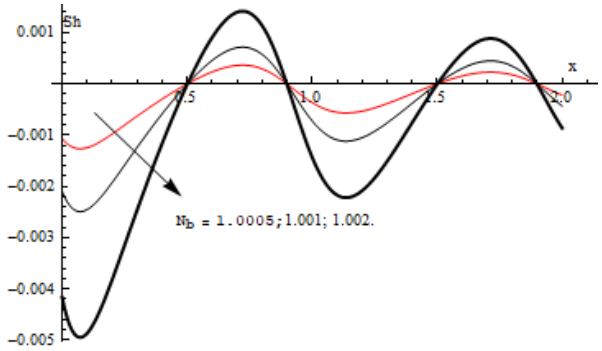

Fig .22 Plots of Sherwood number Sh versus x from Eq. (43) for the effects of N_b.

5. CONCLUSION

The current paper investigates the effect of electro-osmosis on an incompressible MHD peristaltic transport of a nanofluid. The permeability of the fluid, the effects of the Brownian parameter and thermophoresis parameter are taken into account. The analysis is performed under long wavelength and low Reynolds number approximations. The governing equations of motion are analytically solved and the exact solutions of the coupled partial differential equations are obtained. The main results can be epitomized in the following points:

1. A comparison is made between the present results of the fluid velocity by neglecting the electro-osmotic parameter and neglecting the effects of the Hall currents and ion slip and the previous results of Machireddy and Kattamreddy [23]. The results are compared and the comparisons shows a similarity between velocity curves between the present solutions and the previous ones.
2. The trapping bolus are gradually disappearing with the increase of the electro-osmotic parameter (as shown in [18]) and the trapped bolus increases as the Hall parameter is increased.
3. The fluid velocity gives an increasing function of the electro-osmotic parameter (as shown in [12] and [[25]), slip parameter (as shown in [26]), Helmholtz–Smoluchowski velocity (as shown in [12]) and Hall parameter values for large values of the electro-osmotic parameter (as shown in [27]). In contrast, it decreases with the increasing of Hall currents for the small values of the electro-osmotic parameter.
4. The temperature profile increases with the increasing of the thermophoresis parameter and decreases with the increasing of the Brownian parameter.
5. The nanoparticle concentration is an increasing function with the Brownian parameter and the thermophoresis parameter (as shown in [10]).
6. The overwhelming effect of increasing of the elasticity parameters E_1, E_2 and E_3 are raising the magnitude of pressure difference across the channel (as shown in [29]).
7. The volume flow rate enhances with reducing the magnitude of EDL thickness (i.e., the value of the electro-osmotic parameter, $m \in [2,3.3]$) in the interval $x \in [1.2,2]$. Otherwise, these curves are very close to each other (as shown in [21]).
8. The skin friction, the Nusselt number, and Sherwood number have an oscillatory function (as shown in [18]) with the axial axis, due to the peristaltic motion. The skin friction increases by the increase in electro-osmotic parameter and decreases with an increase in the ion slip parameter.
9. The Nusselt number decreases with the increase of thermophoresis parameter, while it increases with the increase of the Brownian parameter and a decrease in Sherwood number occurs with an increase in Brownian parameter and thermophores parameter.

Nomenclature

a	Amplitude.
B_0	Magnetic field.
C	Nanoparticle concentration.
C_0, C_1	Nanoparticle phenomena to the walls of the channel at $y = \eta$ and $-\eta$.
C_v	Coefficient of viscous damping forces.
c_f	Volumetric volume expansion of the fluid.
c_p	Volumetric volume expansion of the particle.
c^*	Phase speed.
d	Mean half width of the channel.
D_B	Brownian diffusion coefficient.
D_T	Thermophoretic diffusion coefficient.
e	The elementary charge.
$\underline{E}$	The electric field.
E_x	The supplied electric field parallel to the channel walls.
E_1, E_2, E_3	Non-dimensional elasticity parameters.
h	Dimensional slip parameter.
K	Permeability of the porous medium.
k	Thermal conductivity of the fluid.
m	Electro-osmotic parameter.
M	Hartman number.
m_1^*	Mass per unit area.
n_+	The number of density of cations charge.
n_-	The number of density of anions.
N_b	Brownian parameter.
N_t	Thermophoresis parameter.
p	Pressure.
p_0	Pressure on the outside surface of the wall due to the tension in the muscles.
Pr	Prandtl number.
Q^*, Q	Dimensional and non-dimensional non-uniformity of channel, respectively.
R	Reynolds number.
T_0, T_1	Temperatures to the walls of the channel at $y = \eta$ and $-\eta$
Sc	Schmidt number.
T	Temperature.
t	Time.
u, v	Components of fluid velocity along x-, y-directions.
U_{HS}	Helmholtz–Smoluchowski velocity

Greek symbols

β	Knudsen number (Slip parameter).
ρ, ρ_p	Density of the fluid and the particle respectively.
ρ_e	Density of the total ionic energy.
γ	Electric permittivity.
ε, δ	Geometric parameters.
ξ	The zeta potential.
λ^*	Wavelength.
λ	Wave speed.
μ	Coefficient of viscosity of the fluid.
υ	Kinematic viscosity.
θ	Dimensionless temperature.
σ	Fluid electrical conductivity.
Ω	Dimensionless nanoparticle concentration.
β_i	The ion slip parameter.
β_e	The Hall parameter.
β^*	The Hall factor.
ψ	Stream function.
ϕ	Electric potential.

REFERENCES

[1] Fung, Y.C. and Yih, C. S., 1968, "Peristaltic transport, Journal of Applied Mechanics," **35** (4), pp. 669–675.

[2] Yin, F. and Fung, Y. C., 1969, "Peristaltic waves in circular cylindrical tubes," Journal of Applied Mechanics ASME, **36,** pp. 579–687.

[3] Misra, J. C. and Maiti, S., 2012, "Peristaltic pumping of blood through small vessels of varying cross section," Journal of Applied Mechanics ASME, **79**(6), pp. 1–19.

[4] Hayat, T., Zahir, H., Alsaedi, A. and Ahmad, B., 2017, "Hall current and Joule heating effects on peristaltic flow of viscous fluid in a rotating channel with convective boundary conditions," Results in Physics, **7,** pp. 2831–2836.

[5] Hayat, T., Rafiq, M. and Alsaedi, A., 2017, "Investigation of Hall current and slip conditions on peristaltic transport of Cu-water nanofluid in a rotating medium," International Journal of Thermal Sciences, **112** (2017) 129–141.

[6] Abdellateef. A. I. and Ul Haque, S. Z., 2016, "Combined Effects of Hall current and heat transfer on peristaltic transport of a nanofluid in a vertical tapered channel through a porous medium," Sultan Qaboos University Journal for Science, 2016, **21**(2), pp. 107–120.

[7] Choi, U. S. and Eastman, J. A., 1995, "Enhancing thermal conductivity of fluids with nanoparticles," ASME International Mechanical Engineering Congress and Exposition, (No. ANL/MSD/CP-84938; CONF-951135-29), San Francisco, pp. 12–17.

[8] Abou-zeid, M. Y., 2015, "Homotopy perturbation method to gliding motion of bacteria on a layer of power-law nanoslime with heat transfer," Journal of Computational and Theoretical Nanoscience, **12,** pp. 3605–3614.

[9] Wang, X. Q. and Mujumdar, A. S., 2007, "Heat transfer characteristics of nanofluids: a review," International Journal of Thermal Sciences, **46,** pp. 1–19.

[10] Mosayebidorcheh, S. and M. Hatami, 2018, "Analytical investigation of peristaltic nanofluid flow and heat transfer in an asymmetric wavy wall channel (Part II: Divergent channel)," International Journal of Heat and Mass Transfer, **126,** pp. 800–808.

[11] Abou-zeid, M. Y., 2018, "Homotopy perturbation method for couple stresses effect on MHD peristaltic flow of a non-Newtonian nanofluid, Microsystem Technologies, **24,** pp. 4839–4846.

[12] Tripathi, D., Sharma, A. and Bég, O. A., 2018, "Joule heating and buoyancy effects in electro-osmotic peristaltic transport of aqueous nanofluids through a microchannel with complex wave propagation," Advanced Powder Technology, **29,** pp. 639–653.

[13] Ranjit, N. K. and Shit, G. C., 2017, "Entropy generation on electro-osmotic flow pumping by a uniform peristaltic wave under magnetic environment," Energy, **128,** pp. 649-660.

[14] Iftikhar, N., Rehman, A., Sadaf, H. and Najam Khan, M., 2018, "Impact of wall properties on the peristaltic flow of Cu-water nano fluid in a non-uniform inclined tube," International Journal of Heat and Mass Transfer, **125,** pp. 772–779.

[15] Hayat, T., Saleem, A., Tanveer, A. and Alsaadi, F, 2017, "Numerical study for MHD peristaltic flow of Williamson nanofluid in an endoscope with partial slip and wall properties," International Journal of Heat and Mass Transfer, **114,** pp. 1181–1187.

[16] Hayat, T., Rafiq, M. and Alsaedi, A., 2017, "Investigation of Hall current and slip conditions on peristaltic transport of Cu-water nanofluid in a rotating medium," International Journal of Thermal Sciences, **112,** pp.129–141.

[17] Ramesh, K., 2016, " Effects of slip and convective conditions on the peristaltic flow of couple stress fluid in an asymmetric channel through porous medium," computer methods and programs in biomedicine, **135,** pp. 1–14.

[18] Moatimid, G. M., Mohamed, M. A., Hassan, M. A. and El-Dakaoky, E. M., 2019, "Electro-osmotic flow and heat transfer of a non-Newtonian nanofluid under the influence of peristalsis," Pramana – Journal of Physics, **90,** pp. 1–14.

[19] Crammer, K. R., 1973, "Magnetofluid dynamics for engineers and applied physicists," Electrical Engineering in Japan, **93** (1), pp. 142–142.

[20] Sutton G. W., and Sherman, A., 1965, "Engineering Magnetohydrodynamics," New York: McGraw-Hill.

[21] Tripathi, D., Bhushan, S., and Bég, O. A., 2017, "Analytical study of electro-osmosis modulated capillary peristaltic hemodynamics," Journal of Mechanics in Medicine and Biology, **17,** pp. 1–22.

[22] Srinivas, S., Gayathri, R. and Kothandapani, M., 2009, "The influence of slip conditions, wall properties and heat transfer on MHD peristaltic transport," Computer Physics Communications, **180** (11), pp. 2115−2122.

[23] Machireddy, G. R. and Kattamreddy, V. R., 2016, "Impact of velocity slip and joule heating on MHD peristaltic flow through a porous medium with chemical reaction," Journal of the Nigerian Mathematical Society, **35**, pp. 227–244.

[24] Ngoma, G. D. and Erchiqui, F., 2006, "Pressure gradient and electroosmotic effects on two

immiscible fluids in a microchannel between two parallel plates," Journal of Micromechanics and Microengineering, **16,** pp. 83–91.

[25] Tripathi, D., Yadav, A., Anwar Bég, O. and Kumara, R., 2018, "Study of microvascular non-Newtonian blood flow modulated by electroosmosis," Microvascular Research, **117,** pp. 28–36.

[26] Ranjit, N. K., Shit, G. C. and Sinha, A., 2017, "Transportation of ionic liquids in a porous micro-channel induced by peristaltic wave with Joule heating and wall-slip conditions," Chemical Engineering Science, **171**, pp. 545–557.

[27] Hayat, T., Asghar, S., Tanveer, A. and Alsaedi, A., 2019, "Effects of Hall current and ion-slip on the peristaltic motion of couple stress fluid with thermal deposition," Neural Computer and Application, **31**, 117–126.

[28] Mekheimer, Kh. S. and Abd elmaboud, Y., 2008, "The influence of heat transfer and magnetic field on peristaltic transport of a Newtonian fluid in a vertical annulus: application of an endoscope," Physics Letters A., **372** (10), pp. 1657-1665.

[29] Ellahi, R., Bhatti M. M. and Pop, I., 2016, "Effects of hall and ion slip on MHD peristaltic flow of jeffrey fluid in a non-uniform rectangular duct," International Journal of Numerical Methods for Heat and Fluid Flow, **26,** pp. 1802–1820.